Spectra of the X#Ray Emission Induced in the Interaction between the Solar Wind and the Heliospheric Gas

The Astrophysical Journal, 617:1347–1352, 2004 December 20

SPECTRA OF THE X-RAY EMISSION INDUCED IN THE INTERACTION BETWEEN THE SOLAR WIND AND THE HELIOSPHERIC GAS

R. Pepino, V. Kharchenko, and A. Dalgarno
Harvard-Smithsonian Center for Astrophysics, 60 Garden Street, Cambridge, MA 02138

and

R. Lallement
Service d'Aéronomie du CNRS, 91371 Verrières-le-Buisson, France
Received 2004 July 6; accepted 2004 August 30

ABSTRACT

Spectra of the heliospheric EUV and X-ray emission induced in the charge transfer collisions of the highly charged solar wind ions with the interstellar gas have been calculated. Cascading photon spectra of individual O^{q+}, C^{q+}, N^{q+}, and Ne^{q+} ions have been constructed using recent data on ion radiative transition probabilities and the state-selective population cross sections for charge transfer collisions of the most abundant heavy solar wind ions with H and He atoms. Emission spectra have been calculated for slow and fast solar winds interacting with the heliospheric H and He gas. Relative intensities of the brightest lines have been predicted. The volume power distribution of the charge transfer EUV and X-ray emission has been computed for simplified models of the solar winds and the interstellar gas. X-ray images of the heliosphere have been composed for the region inside 10 AU from the Sun.

Subject headings: atomic data — solar wind — X-rays: general

Online material: color figures

1. INTRODUCTION

The discovery of X-rays from comets (Lisse et al. 1996) and the identification of the mechanism as charge transfer in collisions of highly charged ions of the solar wind with the neutral molecules of the cometary atmospheres (Cravens 1997, 2002) led to the suggestion (Cox 1998) that charge transfer of solar wind ions interacting with the interstellar hydrogen and helium atoms flowing into the heliosphere contributes to the soft X-ray background and may be responsible for the long-term enhancements (LTEs) seen with *ROSAT* (Snowden et al. 1994). A local source of X-rays is consistent with the observed correlation of LTEs with solar activity (Freyberg 1998; Cravens et al. 2001; Robertson et al. 2001). Estimates of the absolute intensity by Cravens (2000) indicate that the heliospheric X-rays may provide a significant fraction of the measured soft X-ray background. An additional local source of soft X-rays, charge transfer collisions of the heavy solar wind ions with the geocoronal hydrogen gas, has been investigated theoretically (Robertson & Cravens 2003a, 2003b) and has been detected recently in *Chandra* X-ray observations of the dark Moon (Wargelin et al. 2004).

Sky maps have been constructed of the total emission of heliospheric X-rays by Robertson & Cravens (2003a, 2003b) and Lallement (2004) and of the 30.4 nm line of He^+ produced by charge transfer of solar wind alpha particles by Gruntman (2001). We present here predictions of the X-ray spectra in the heliosphere as well as maps of the volume emission intensity corresponding to the slow and fast solar wind. We distinguish between charge transfer to neutral hydrogen atoms and neutral helium atoms, and we provide estimates of the efficiency factors (Cravens 1997) that characterize the X-ray intensities.

2. HYDROGEN AND HELIUM DENSITY MAPS AND THE SOLAR WIND

Neutral hydrogen and helium atoms flow into the heliosphere from the interstellar medium and are converted to positive ions by photoionization by the solar ultraviolet radiation and by charge transfer with solar wind protons and alpha particles. There are many models of the resulting distribution of hydrogen and helium atoms (Fahr 1973; Holzer 1977; Lallement et al. 1993; Baranov et al. 1998; Fahr et al. 2000; Zank 1999; Zank & Muller 2003). The X-ray intensities vary with solar activity through changes in the distributions of the ionized and neutral helium and hydrogen and in the solar wind flux and composition. We adopt a simple trajectory hot model (Lallement 2004) appropriate for solar maximum for which the helium atom flow velocity is 25.5 km s^{-1}, the helium temperature is 7000 K (Witte et al. 2004), the hydrogen velocity is 22 km s^{-1}, and the hydrogen temperature is 11,000 K (Costa et al. 1999). The model does not take into account the density increase at the edge of the heliosphere, the hydrogen wall, which lies beyond the region of our maps.

There are two kinds of solar winds: a variable slow wind with a velocity ranging from 300 to 600 km s^{-1} and a fast wind with a velocity between 600 and 800 km s^{-1} (Smith et al. 2003). For our models we follow Robertson & Cravens (2003a) and adopt a slow wind at solar latitudes less than 20° with a proton density of $6.5/r^2$ cm^{-3} and a velocity of 450 km s^{-1} and a fast wind at latitudes greater than 20° with a proton density of $3.2/r^2$ cm^{-3} and a velocity of 750 km s^{-1}, where r is the radial distance from the Sun in AU. The boundary surface between the fast and slow solar winds has a wavelike structure and varies with time. The X-ray flux may vary strongly with heliospheric latitude, and a sharp transition may be apparent in the antisolar direction at any particular time. The time-averaged boundary will be less sharp than that in our simplified model. We took the fractional abundances listed by Schwadron & Cravens (2000) as typical heavy ion charge compositions for the slow and fast winds.

3. CHARGE TRANSFER SPECTRA

Multiply charged ions traversing a gas capture electrons from the neutral atoms and molecules into highly excited states giving rise to a radiative cascade of emission lines in the X-ray

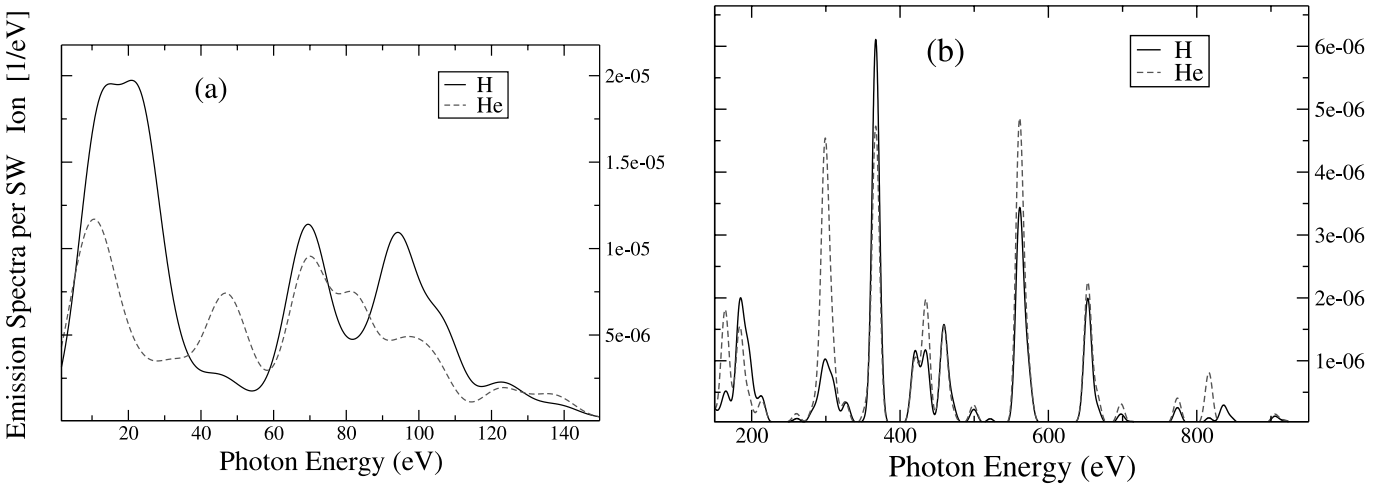

FIG. 1.—(*a*) Predicted spectra of the EUV and soft X-ray emission induced by heavy ions of the slow solar wind colliding with hydrogen and helium. The number of photons is normalized to a single solar wind ion, and the photon energy resolution is taken as 12 eV. Emission lines produced in charge transfer collisions of He^{2+} solar wind ions are not included. (*b*) Spectra of X-ray emission for heavy ions of the slow solar wind colliding with hydrogen and helium. [*See the electronic edition of the Journal for a color version of this figure.*]

and ultraviolet region of the spectrum (Cravens 2000). In collisions with multielectron systems, double capture may occur. It is followed by Auger ionization, in which the ion gains only one electron, or by radiative stabilization, in which the ion gains two electrons (Kamber et al. 1999; Greenwood et al. 2000, 2001; Hasan et al. 2001; Gao & Kwong 2002; Beiersdorfer et al. 2003). Rigazio et al. (2002) have described a semiempirical procedure with which they obtain, for a given ion in a specific gas, a set of entry rates into the individual excited states that reproduces the experimental X-ray spectrum after cascading. We have applied their procedure to construct a database (R. Pepino et al. 2004, in preparation) of the transition energies and relative strengths of the individual emission lines that are produced by charge transfer of the ions in the solar wind. When averaged over the laboratory energy resolution, the spectrum reproduces the measurements. There are no laboratory data for the solar wind ions of iron, magnesium, silicon, and sulfur. For these we follow the prescription of Kharchenko & Dalgarno (2001). The approximation limits the accuracy of the predictions of the detailed spectra below 350 eV but introduces little uncertainty in the calculations of the total emitted energy.

The number of photons with energy E_j emitted in a collision of a solar wind ion i with density n_i with a neutral species x can be written

$$N_{x,i}(E_j) = \frac{n_i \sigma_i^x}{\sum_i n_i \sigma_i^x}\ \gamma_{ij}^x, \tag{1}$$

where σ_i^x is the capture cross section for the heavy solar wind ion i and γ_{ij}^x is the yield of photons with energy E_j emitted in the collision of ions i with atom x. The factor $n_i\sigma_i^x / \sum_i n_i \sigma_i^x$ is the relative frequency of electron capture by the heavy solar wind ion i. The numbers of photons are normalized to a single solar wind ion by multiplying $N_{x,i}(E_j)$ by the relative fraction ξ of highly charged ions in the solar wind flux, $\tilde{N}_{x,i}(E_j) = \xi N_{x,i}(E_j)$. We adopted $\xi = 1.04\ 10^{-3}$ for the slow solar wind and $\xi = 1.2\ 10^{-3}$ for the fast wind (Schwadron & Cravens 2000).

The spectra $\tilde{N}_{\mathrm{H},i}(E_j)$ and $\tilde{N}_{\mathrm{He},i}(E_j)$, resulting from collisions of the heavy solar wind ions with hydrogen and helium atoms obtained by summing over i, j in equation (1), are illustrated in Figures 1*a*–2*b* for the slow and fast winds. These spectra do

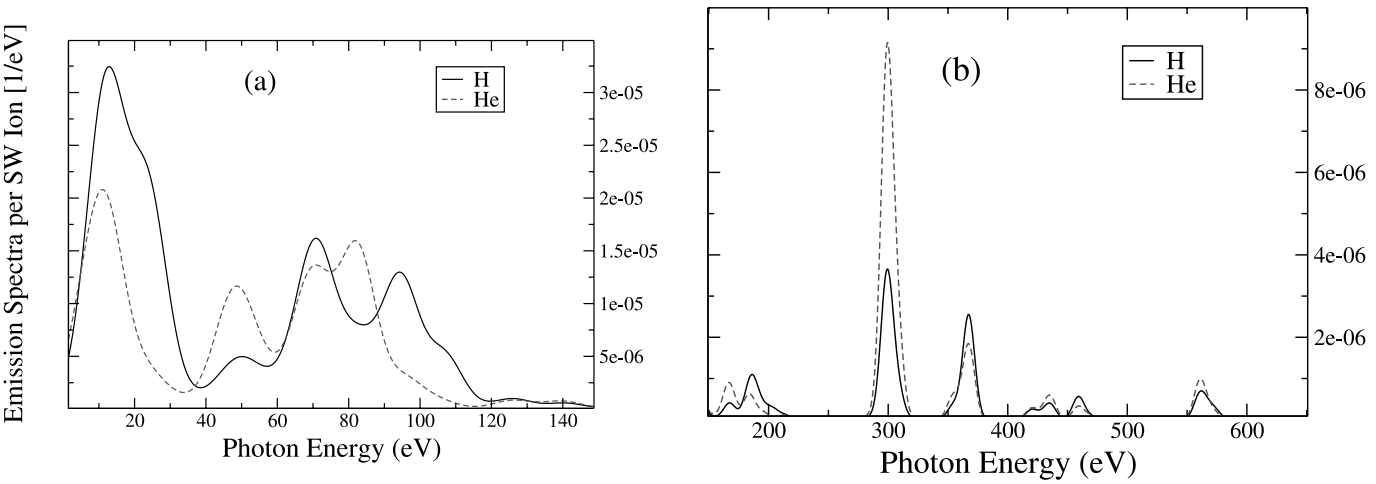

FIG. 2.—(*a*) Predicted EUV and soft X-ray spectra from heavy ions of the fast solar wind colliding with hydrogen and helium. Spectra induced by He^{2+} solar wind ions are not included. (*b*) Predicted X-ray spectra from heavy ions of the fast solar wind colliding with the hydrogen and helium gases. [*See the electronic edition of the Journal for a color version of this figure.*]

TABLE 1

NUMBER OF PHOTONS $\tilde{N}_{\mathrm{H},i}(E_j)$ AND $\tilde{N}_{\mathrm{He},i}(E_j)$ OF THE MAJOR X-RAY EMISSION FEATURES

TRANSITION	ENERGY (eV)	SLOW SOLAR WIND		FAST SOLAR WIND	
		H	He	H	He
C^{4+} $(1s2s^3S \rightarrow 1s^2\,{}^1S)$	299	1.0×10^{-5}	5.0×10^{-5}	4.2×10^{-5}	1.0×10^{-4}
C^{4+} $(1s2p^3P \rightarrow 1s^2\,{}^1S)$	304	7.1×10^{-7}	4.4×10^{-6}	2.7×10^{-6}	8.8×10^{-6}
C^{4+} $(1s2p^1P \rightarrow 1s^2\,{}^1S)$	308	1.5×10^{-6}	1.0×10^{-5}	3.8×10^{-7}	2.0×10^{-5}
C^{5+} $(2p \rightarrow 1s)$	367	7.6×10^{-5}	5.9×10^{-5}	3.1×10^{-5}	2.3×10^{-5}
N^{5+} $(1s2s^3S \rightarrow 1s^2\,{}^1S)$	420	1.3×10^{-5}	1.2×10^{-5}	2.9×10^{-6}	3.3×10^{-6}
N^{5+} $(1s2p^3P \rightarrow 1s^2\,{}^1S)$	426	2.1×10^{-6}	1.4×10^{-6}	5.0×10^{-7}	4.7×10^{-7}
N^{5+} $(1s2p^1P \rightarrow 1s^2\,{}^1S)$	431	2.1×10^{-6}	1.6×10^{-6}	5.1×10^{-7}	5.3×10^{-7}
C^{5+} $(3p \rightarrow 1s)$	435	1.3×10^{-5}	2.3×10^{-5}	4.6×10^{-6}	7.0×10^{-6}
C^{5+} $(4p \rightarrow 1s)$	459	1.9×10^{-5}	1.9×10^{-5}	7.0×10^{-6}	4.1×10^{-6}
O^{6+} $(1s2s^3S \rightarrow 1s^2\,{}^1S)$	561	4.0×10^{-5}	5.8×10^{-5}	7.8×10^{-6}	1.2×10^{-5}
O^{6+} $(1s2p^3P \rightarrow 1s^2\,{}^1S)$	568	8.2×10^{-6}	9.1×10^{-6}	2.5×10^{-6}	1.9×10^{-6}
O^{6+} $(1s2p^1P \rightarrow 1s^2\,{}^1S)$	574	6.4×10^{-6}	6.8×10^{-6}	2.1×10^{-6}	1.4×10^{-6}
O^{7+} $(2p \rightarrow 1s)$	653	2.5×10^{-5}	3.0×10^{-5}	...	...
O^{7+} $(4p \rightarrow 1s)$	816	1.2×10^{-6}	1.0×10^{-5}	...	...

not include emissions at 40.8 eV and near 21.2 eV because of capture by alpha particles. They are discussed by Gruntman (2001) for the solar wind interacting with the heliospheric gas and by Bodewits et al. (2004) for the cometary environment. The spectra also exclude emissions from the small fraction of heavier ions Fe^{q+}, S^{q+}, and Si^{q+}. They are included in calculations of the total emission power. The emission of the lithium-like Mg^{9+} ions, excited in collisions of the relatively abundant Mg^{10+} solar wind ions (Schwadron & Cravens 2000), is taken into account in the computed spectra. The line profiles in Figures 1*a*–2*b* are represented by Gaussian functions with a FWHM of 12 eV, which is within the experimental spectroscopic resolution for microcalorimeter detections of X-rays by McCammon et al. (2002). There are significant differences between the spectra arising from charge exchange with hydrogen and helium and between the slow and fast winds. The large difference in the ionization potentials of hydrogen and helium atoms has a substantial effect on the distributions of energy levels populated by charge transfer and their variation with velocity. The predicted number of photons of the most intense emission features is listed in Table 1. For the slow wind the mean number of photons emitted with energies above 100 eV in collisions with hydrogen is 8.9×10^{-4} with a mean energy of 294 eV, and for collisions with helium the mean number is 6.9×10^{-4} with a mean energy of 308 eV. For the fast wind the corresponding values are 3.2×10^{-4} and 252 eV for hydrogen and 3.6×10^{-4} and 276 eV for helium. In collisions with hydrogen, the total energy emitted in emission lines above 100 eV is a factor of 6.7 times the energy emitted in the feature composed of the helium-like triplet of O^{6+} at 560.9, 568.5, and 574.0 eV for the slow wind and 12 for the fast wind. The factors for helium are 6 and 13, respectively.

The ratios of intensities of the triplet $2^3S - 1^1S$ and $2^3P - 1^1S$ lines and the singlet $2^1P - 1^1S$ line of helium-like ions provide a potentially valuable probe of the excitation mechanism. We estimated the relative contributions of singlet and triplet transitions of the helium-like ions by combining theoretical calculations with the measurements of Greenwood et al. (2001) and Hasan et al. (2001). There is some uncertainty in the derived ratios because the experiments of Greenwood et al. (2000, 2001) do not capture the emissions from the long-lived metastable states. For capture from hydrogen, we find a ratio of the summed intensity of the $2^3S \rightarrow 1^1S$ and $2^3P \rightarrow 1^1S$ lines compared to the $2^1P \rightarrow 1^1S$ line of 6.7 for O^{6+}, 7.3 for N^{5+}, and 6.8 for C^{4+}. For helium, the ratios are 7.7, 8.6, and 5.3 for O^{6+}, N^{5+}, and C^{4+}, respectively. High resolution would be necessary to distinguish between capture from hydrogen and capture from helium.

The emissivity of X-rays with energies greater than 100 eV from the interstellar gas is given by

$$I = \sum_{i,j} I_i(E_j > 100 \text{ eV}), \tag{2}$$

where

$$I_i(E_j) = v n_{\mathrm{sw}} \left[n_{\mathrm{H}} \langle \sigma_{\mathrm{H}} \rangle N_{\mathrm{H},i}(E_j) + n_{\mathrm{He}} \langle \sigma_{\mathrm{He}} \rangle N_{\mathrm{He}}(E_j) \right] E_j \tag{3}$$

and v is the solar wind velocity, $n_{\mathrm{sw}} = \sum_i n_i$ is the total density of heavy solar wind ions, $\langle \sigma_x \rangle = \sum_i n_i \sigma_i^x / n_{\mathrm{sw}}$ is the average charge transfer cross section for heavy solar wind ions in hydrogen or helium gas, and n_{H} and n_{He} are the heliospheric hydrogen and helium number densities. Following Cravens (1997) we introduce efficiency factors α_{H} and α_{He}, defined by

$$\alpha_{\mathrm{H}} = \frac{n_{\mathrm{sw}}}{n_p} \langle \sigma_{\mathrm{H}} \rangle \sum_{i,j} N_{\mathrm{H},i}(E_j) E_j, \tag{4}$$

$$\alpha_{\mathrm{He}} = \frac{n_{\mathrm{sw}}}{n_p} \langle \sigma_{\mathrm{He}} \rangle \sum_{i,j} N_{\mathrm{He},i}(E_j) E_j, \tag{5}$$

where n_p is the total density of solar wind ions, including protons and alpha particles. Then

$$I = v n_p (n_{\mathrm{H}} \alpha_{\mathrm{H}} + n_{\mathrm{He}} \alpha_{\mathrm{He}}). \tag{6}$$

We find that, for the O^{q+}, C^{q+}, N^{q+}, Ne^{q+}, and Mg^{10+} solar wind ion abundances of Schwadron & Cravens (2000), $\alpha_{\mathrm{H}} = 9.38 \times 10^{-16}$ eV cm^2 and $\alpha_{\mathrm{He}} = 4.32 \times 10^{-16}$ eV cm^2 for the slow solar wind and $\alpha_{\mathrm{H}} = 3.33 \times 10^{-16}$ eV cm^2 and $\alpha_{\mathrm{He}} = 1.75 \times 10^{-16}$ eV cm^2 for the fast solar wind. The emissions of heavier ions Fe^{q+}, S^{q+}, and Si^{q+}, which radiate photons with energies below 300 eV, increase the values of α by 25% for the slow solar wind and 19% for the fast wind. Robertson & Cravens (2003a) adopted $\alpha_{\mathrm{H}} = 6 \times 10^{-16}$ eV cm^2 and $\alpha_{\mathrm{He}} = 3 \times 10^{-16}$ eV cm^2 in their discussion of the geocoronal and heliospheric X-rays.

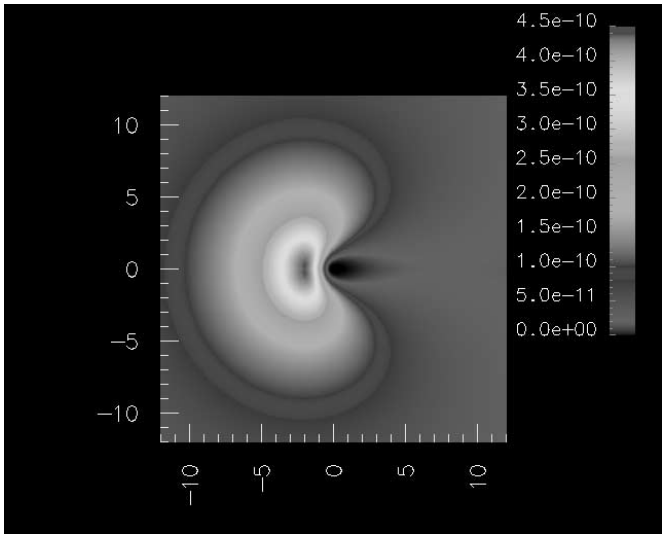

FIG. 3.—Power density generated by solar wind ions from the interstellar hydrogen gas in the ecliptic plane. The color distribution indicates the volume power in eV s^{-1} cm^{-3}. Distances from the Sun (0, 0) are shown in AU. [*See the electronic edition of the Journal for a color version of this figure*.]

Figures 3–5 are maps of the total luminosity I at positions (X, Y) in the ecliptic plane between ± 12 AU from the Sun, with the Sun as the origin of coordinates. In these figures, the interstellar gas is traveling from left to right and downward at an angle of 6° with respect to the ecliptic plane (Robertson & Cravens 2003a). The heliospheric neutral hydrogen and helium distribution corresponds to the time of the *ROSAT* survey as derived by Lallement (2004), and the wind is the slow solar wind.

The crescent shape in Figure 3 is similar to the X-ray image observed from comets (Lisse et al. 1996). It is a consequence of the r^{-2} dependence of the solar wind flux and the spatial density of hydrogen. The absence of X-ray emission near the Sun is due to the loss of hydrogen atoms by ionization, whereas its absence near the cometary nucleus is due to neutralization of the solar wind ions. Figure 4 has a tail on the downwind side of the Sun that is a reflection of the helium cone caused by gravitational focusing (Michels et al. 2002; Lallement 2004).

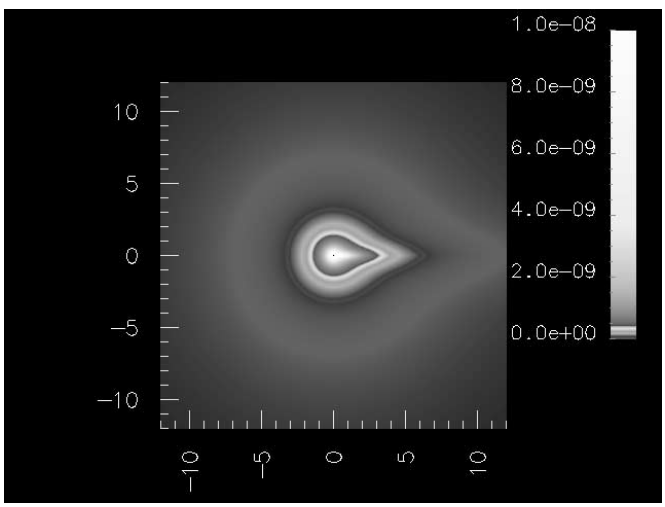

FIG. 4.—Power density generated from the interstellar helium gas in the ecliptic plane. Distances are measured in AU from the Sun as origin of coordinates. [*See the electronic edition of the Journal for a color version of this figure*.]

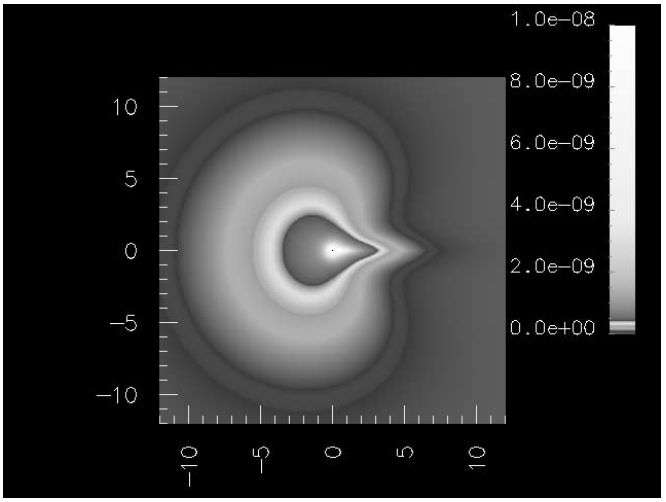

FIG. 5.—Power density generated from both hydrogen and helium in the ecliptic plane. [*See the electronic edition of the Journal for a color version of this figure*.]

Figure 5 is a superposition of Figures 3 and 4 and is a map of the total emissivity of the heliosphere. The luminosity obtained by integrating I over a sphere of radius 10 AU around the Sun is 2.1×10^{14} W.

Figure 6 is a map of the emissivity in a plane perpendicular to the ecliptic plane. The ecliptic plane is the (X, Z) plane with the Z-axis pointing out of the page, and the interstellar wind moves from left to right traveling 6° downward with respect to the Y-axis. The figure illuminates the contrast between the emission in the slow and fast solar wind regions, which occurs primarily as a result of the differences in relative ion abundances in the slow and fast solar wind, the solar wind velocity itself playing a minor role.

In order to illustrate the spectral differences between the slow and fast solar wind regions, we present maps of the brightest emission lines of O^{7+} (653, 774, and 836 eV) and O^{6+} (561, 569, and 574 eV) in Figures 7*a* and 7*b*. The lack of emission in the fast solar wind region in Figure 7*a* is due to the absence of O^{8+} in the fast solar wind (Schwadron & Cravens 2000).

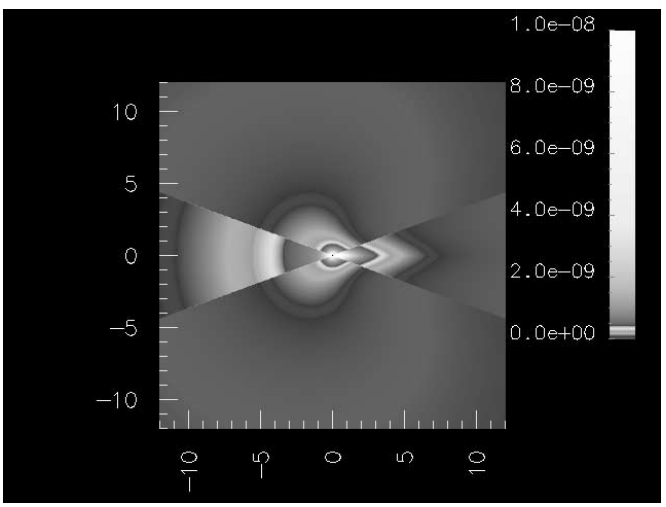

FIG. 6.—Power density generated from both hydrogen and helium in the plane defined by the heliospheric polar axis and the direction of the incoming interstellar gas. [*See the electronic edition of the Journal for a color version of this figure*.]

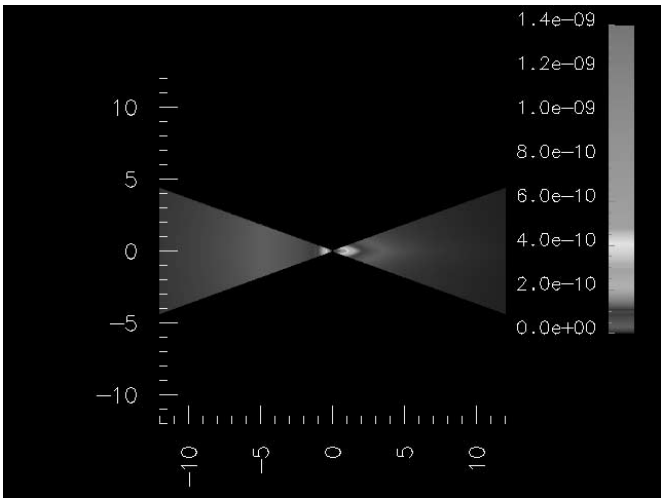

FIG. 7*a*

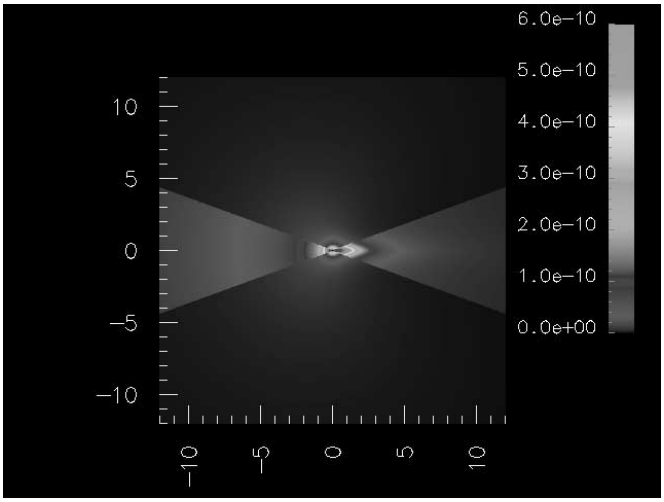

FIG. 7*b*

FIG. 7.—Power density generated in the plane of the heliospheric polar axis and the interstellar gas velocity by individual solar wind ions (excited O^{7+} ions in panel *a* and excited O^{6+} ions in panel *b*). [*See the electronic edition of the Journal for a color version of this figure*.]

The satellite measurements of X-ray emission provide information on the directional intensities $J_d(\boldsymbol{r}_0, \boldsymbol{e})$, where $\boldsymbol{r}_0$ is the heliospheric position of the satellite detector and $\boldsymbol{e}$ is the unit vector along a line of sight. Values of the directional intensities can be obtained by integration along the line of sight of the X-ray emissivity given by equation (6),

$$J_d(\boldsymbol{r}_0, \boldsymbol{e}) = \int_0^\infty I(\boldsymbol{r}_0 + \boldsymbol{e}s)\, ds. \tag{7}$$

Heliospheric maps of X-ray emission induced by the solar wind have been constructed recently with approximate values of the emission yield coefficients $\alpha_{\rm H}$ and $\alpha_{\rm He}$ (Robertson & Cravens 2003a; Lallement 2004). We have calculated the line-of-sight X-ray intensities for several heliospheric directions and X-ray detector positions. At the highest upwind position, where the longitudinal angle of the Earth in ecliptic coordinates is around 255°, the intensity of X-ray emission in the upwind direction is computed to be 12.3 keV cm^{-2} s^{-1}, about 20% of it originating from the heliospheric He gas. If observations are conducted in a direction perpendicular to the wind velocity, the intensities are 12.1 keV cm^{-2} s^{-1} for the ecliptic plane and 4.2 keV cm^{-2} s^{-1} for the direction toward the northern heliospheric pole. The contributions from the He gas are 30% and 38%, respectively, higher than those in the upwind direction.

Observations from the lowest downwind position at the longitudinal angle of the Earth of 74°.5 would yield the downwind X-ray intensity of 14.2 keV cm^{-2} s^{-1} with about 80% of the emission arising in the He cone. For directions perpendicular to the wind the intensity near the ecliptic plane is 47 keV cm^{-2} s^{-1}, and for the direction to the northern pole it is 6.4 keV cm^{-2} s^{-1}. The emission from the He cone contributes more than 80% of the total intensity. The directional intensities calculated with our α values are 20%–60% larger in the regions of the slow solar wind and 30%–50% smaller in the regions of the fast wind than values presented in recent calculations (Robertson & Cravens 2003a; Lallement 2004), if the same distributions of heliospheric gas are used.

4. CONCLUSIONS

We have calculated the soft X-ray emission spectrum arising from the charge transfer collisions of solar wind ions with heliospheric hydrogen and helium atoms. The spectra for hydrogen and helium collisions may be distinguished by their different spatial distributions, and measurements of the difference are potentially important tests of the charge transfer mechanism. The efficiency of excitation in collisions with hydrogen is twice that in collisions with helium for both the fast and slow winds.

The X-ray emission power of the slow solar wind is about 3 times larger than that of the fast solar wind; thus, regions of the heliosphere occupied by the slow solar wind are sources of more intense radiation than are the fast solar wind regions.

The computed maps of X-ray brightness show the helium cone and a crescent shape formed by the hydrogen gas. The heliospheric images depend on the energies of the photons.

The results of investigations of the spectra and morphology of the heliospheric X-rays can be used for the analysis of X-ray emissions induced by stellar winds from astrospheres (Wargelin & Drake 2001), and, if detected, the spectral features of astrospheric X-rays would provide a diagnostic of the stellar wind composition.

We are grateful to Jason Greenwood for laboratory data on ion emission spectra of solar wind ions and to Phillip Stancil for providing detailed information on the charge transfer cross sections. This work has been supported by the NASA Solar and Heliospheric Physics grant NNG04GD57G. A. D. has been supported by the NASA Office of Space Science grant NAG5-13331.

REFERENCES

Baranov, V. B., Izmodenov, V. V., & Malama, Y. G. 1998, J. Geophys. Res., 103, 9575
Beiersdorfer, P., et al. 2003, Science, 300, 1558
Bodewits, D., Juhasz, Z., Hoekstra, R., & Tielens, A. G. G. M. 2004, ApJ, 606, L81
Costa, J., Lallement, R., Quemerais, E., Bertaux, J. L., Kyrola, E., & Schmidt, W. 1999, A&A, 349, 660
Cox, D. P. 1998, in The Local Bubble and Beyond, ed. D. Breitschwerdt, M. J. Freyberg, & J. Trümper (Berlin: Springer), 121

Cravens, T. E. 1997, Geophys. Res. Lett., 24, 105
———. 2000, ApJ, 532, L153
———. 2002, Science, 296, 1042
Cravens, T. E., Robertson, I. P., & Snowden, S. L. 2001, J. Geophys. Res., 106, 24883
Fahr, H. J. 1973, Space Sci. Rev., 15, 483
Fahr, H. J., Kausch, T., & Scherer, H. 2000, A&A, 357, 268
Freyberg, M. J. 1998, Astron. Nachr., 319, 93
Gao, H., & Kwong, V. H. S. 2002, ApJ, 567, 1272
Greenwood, J. B., Williams, I. D., Smith, S. J., & Chutjian, A. 2000, ApJ, 533, L175
———. 2001, Phys. Rev. A, 63, 062707
Gruntman, M. 2001, J. Geophys. Res., 106, 8205
Hasan, A. A., Eissa, F., Ali, R., Schults, D., & Stancil, P. C. 2001, ApJ, 560, L201
Holzer, T. E. 1977, J. Geophys. Res., 82, 23
Kamber, E. Y., Abdallah, M. A., Cocke, C. L., & Stockli, M. 1999, Phys. Rev. A, 60, 2907
Kharchenko, V., & Dalgarno, A. 2001, ApJ, 554, L99
Lallement, R. 2004, A&A, 418, 143
Lallement, R., Bertaux, J. L., & Clarke, J. T. 1993, Science, 260, 1095
Lisse, C. M., et al. 1996, Science, 274, 205
McCammon, D., et al. 2002, ApJ, 576, 188
Michels, J. G., et al. 2002, ApJ, 568, 385
Rigazio, M., Kharchenko, V., & Dalgarno, A. 2002, Phys. Rev. A, 66, 064701
Robertson, I. P., & Cravens, T. E. 2003a, J. Geophys. Res., 108, LIS6
———. 2003b, Geophys. Res. Lett., 30, 22
Robertson, I. P., Cravens, T. E., Snowden, S., & Linde, T. 2001, Space Sci. Rev., 97, 401
Schwadron, N. A., & Cravens, T. E. 2000, ApJ, 544, 558
Smith, E. J., et al. 2003, Science, 302, 1165
Snowden, S. L., McCammon, D., Burrows, D. N., & Mendenhall, J. A. 1994, ApJ, 424, 714
Wargelin, B. J., & Drake, J. J. 2001, ApJ, 546, L57
Wargelin, B. J., Markevitch, M., Juda, M., Kharchenko, V., Edgar, R., & Dalgarno, A. 2004, ApJ, 607, 596
Witte, M., et al. 2004, Adv. Space Res., 34, 61
Zank, G. P. 1999, Space Sci. Rev., 89, 413
Zank, G. P., & Muller, H. R. 2003, J. Geophys. Res., 108, SSH7